Powder Technology 394 (2021) 1017–1025

Contents lists available at ScienceDirect

Powder Technology

journal homepage: www.elsevier.com/locate/powtec

Porous biochar/heptadecane composite phase change material with leak-proof, high thermal energy storage capacity and enhanced thermal conductivity

Gökhan Hekimoğlu [a,*], Ahmet Sarı [a,b,*], S. Arunachalam [c], Hasan Arslanoğlu [d], Osman Gencel [e]

[a] Department of Metallurgical and Material Engineering, Karadeniz Technical University, 61080 Trabzon, Turkey
[b] King Fahd University of Petroleum and Minerals, Centers of Research Excellence, Renewable Energy Research Institute, Dhahran, 31261 Saudi Arabia
[c] Department of Green Energy Technology, Madanjeet School of Green Energy Technologies, Pondicherry University, Puducherry 605014, India
[d] Kırşehir Ahievran University, Engineering Faculty, Chemical and Process Engineering, Kırşehir, Turkey
[e] Bartin University, Department of Civil Engineering, 74100 Bartin, Turkey

ARTICLE INFO

Article history:
Received 15 April 2021
Received in revised form 7 August 2021
Accepted 13 September 2021
Available online 15 September 2021

Keywords:
Waste lemon peel
Bio-char
Heptadecane
PCM
Thermal energy storage
Thermal conductivity

ABSTRACT

Solid-liquid phase change materials (PCMs) have been preferred for solar passive thermal energy storage (TES) applications. However, low thermal conductivity and leakage issue of molten PCMs considerably restrain their TES potential. In this framework, n-Heptadecane (HD) as a solid-liquid PCM was incorporated with carbonized lemon peel (CLP) for development of a novel leak-proof composite PCM. Chemical compatibility between the constituents of the leak-proof composite PCM was examined by using FTIR spectroscopy and XRD diffraction analyses. The DSC results revealed that the developed leak-proof CLP/HD composite PCM had a melting temperature of 19.79 °C and LHS capacity of 141.8 J/g. The composite PCM exposed venerable thermal degradation stability after a 1000-cycling heating-cooling process. Thermal conductivity of the CLP/HD composite PCM (0.46 W/m.K at 10 °C) was measured as approximately 77% higher than that of pristine HD (0.26 W/m.K at 10 °C).

1. Introduction

Global energy requirement is growing alarmingly because of rapid urbanization, industrial development and high living standards. Efficient and affordable energy storage systems are required to save energy and minimize the reliance on fossil fuels and to diminish the adverse effect on the environment. Thermal energy storage (TES) can provide these benefits when combined with renewable energy sources and technologies. Such a system comprises of sensible, latent and thermochemical heat storage [1–3]. Latent heat storage (LHS) using phase change materials (PCMs) is more preferred than sensible heat storage because of isothermal phase change and high energy density and long term durability. PCMs serve as potential energy saving materials in various TES implementations including thermal controlling of buildings, recovery of waste heat, cooling of electronic gadgets, solar power utilization etc. [4–6]. PCMs can minimize the temperature fluctuations in buildings by absorbing heat when the outdoor temperature is higher than inside room temperature and also releases the stored heat as the outdoor temperature is become lower. Therefore, they can stabilize the building inside temperature and reduce energy load needed for heating and cooling of building [7]. Solid-liquid PCMs have categorically identified as paraffins, hydrated salts, fatty acids, fatty alcohols, organic esters and some polymers [8]. The leakage issue of molten PCM and low thermal conductivity are main foremost shortcomings encountered during their practice implementations [9]. Although great attempts have been undertaken for solving these problems, it remains a challenge to develop PCMs with desired operating temperature, high LHS capacity, relatively high thermal conductivity, and good cycling thermal/and chemical stability and low-cost [10]. The integration of PCMs with porous, lightweight and cost-effective carrier materials is one of the most preferred methods for effective solving the problems [11,12]. Within this outline, several form-stable or shape stabilized composites have been developed by incorporating the PCMs with different kind of supporting matrices such as silica fume [13], palygorskite [14], diatomite [15] and vermiculite [16] etc. Most of the form-stable composite PCMs possess poor thermal conductivity and therefore they have been doped with some carbon based fillers with relatively high thermal conductivity such as graphene, graphene oxide, carbon nanotube and carbon nanofiber [17]. However,

* Corresponding authors.
E-mail addresses: ghekimoglu@ktu.edu.tr (G. Hekimoğlu), ahmet.sari@ktu.edu.tr (A. Sarı).

https://doi.org/10.1016/j.powtec.2021.09.030
0032-5910/

high-cost and the agglomeration drawbacks considerably limit their preference for TES systems.

On the other hand, bio-waste derived bio-chars can be seen as good candidates to replace the above-mentioned carbon fillers due to the possibility of being produced cheaper and environmentally friendly [18,19]. Therefore, they have been used used for eradicating leakage difficulty as well as enhancing the thermal conductivity of PCMs because of good surface textural properties [20–22]. Wang et al. [23] searched the porosity effect of expanded graphite and activated carbon on the energy storage performance of PEG as PCM. Zhao et al. [24] fabricated composite PCM by incorporating PEG with bio-carbons derived from fresh potatoes and white radish and also reported that the produced composite PCM kept its LHS characteristics of even after 200 melt/freeze cycles. Atinafu et al. [25] prepared three kinds of bio-chars for shape stabilizing n-dodecane and 1-dodecanol and concluded that the developed composites exhibited a LHS capacity of 90 and 73 J/g, respectively. Feng et al. [26] syntheized a shape-stable PEG/mesoporous carbon composite via vaccum impregnating technique. Nicholas et al. [27] impregnated n-octadecane with oil palm waste shell derived bio-char for thermal regulation studies. Chen et al. [28] produced form-stable PCMs consisted with lauric acid and activated carbon (AC) with increased thermal conductivity and stability. Zhang et al. [29] impregnated lauric acid-stearic acid eutectic PCM with corn cob derived- carbon, which had 87% higher thermal conductivity than that of the eutectic PCM. Xu et al. [30] integrated paraffin with orange-peel based bio-char, which was resulted in a leak-proof composite PCM with good thermal reliability. Wen et al. [31] loaded the melted stearic acid to sunflower straw-based carbon and proposed it for TES implementations.

Turkey is one among the world's largest lemon growers with an estimated annual production of 1.1 million tons per year. The lemon peel has been evaluated to produce low-cost, porous and ecofriendly bio-char for removal of organic and inorganic pollutant [32–34]. The present work was intended to produce carbonized lemon peel (CLP) as effective carrier matrix and then used to build a leak-proof composite PCM with boosted thermal conductivity and LHS capacity. The extensive literature survey revealed that no study have been carried out about the evaluation of CLP scaffold for developing a leak-proof composite PCM. N-heptadecane (HD) was chosen as PCM because of its appropriate melting temperature (21–22 °C) and LHS capacity (216–217 J/g) for thermal management of buildings [35–37]. To address the molten leakage and low thermal conductivity shortcomings of HD, it was successfully impregnated into the pores of the CLP framework via vacuum technique. The morphology, chemical/and crystal structures, LHS properties, thermal degradation stability, cycling LHS reliability and thermal conductivity of the leak-proof CLP/HD composite were investigated systematically for the first time in this work. The impacts of the improved thermal conductivity on the reducing melting and solidification times of the HD and the CLP/HD composite were also estimated comparatively. The present study demonstrated that the developed leak-proof composite PCM can be utilized as green admixture for manufacturing novel energy-saving building materials because of its appreciated TES characteristics.

2. Experimental

2.1. Material

Heptadecane (HD; chemical formula: $CH_3(CH_2)_{15}CH_3$; molecular weight: 240.48 g/mol; assay: ≥98.0%; density: 0.78 g/cm^3 at 20 °C; melting point: 22 °C) was supplied from Sigma-Aldrich Company. The lemon samples were obtained from Mediterranean region of Turkey.

2.2. Preparation of carbonized lemon peel (CLP)

A carbonized lemon pulp (CLP) material was obtained by modifying the cellulosic and pectic substances in the skin of the lemon with citric acid in the juice of the lemon. The thin yellow outer skin of the washed lemons was grated and removed. After the juice was squeezed, the peel of the lemon was cut into 3–5 mm pieces and dried. The lemon juice was filtered through ordinary filter paper and the seeds and coarse fibers were separated. Dried lemon peel pieces were mixed with lemon juice on a glass tray and left to absorb the water. After the coarse water was removed using a fan in the open air, it was dried at 50 °C overnight. It was then heated in an oven at 180 °C for 1 h in a nitrogen atmosphere. The dark colored material ground in a coffee grinder was sieved through a 100 mesh sieve. In order to remove excess citric acid, the resulting powder was washed with distilled water. The washing process was continued with the lead nitrate solution until the wash water did not precipitate lead citrate. The CLP obtained by filtration was dried at 100 °C and used in experiments. The schematic demonstration of the production procedure of the CLP was given in Fig. 1.

2.3. Fabrication of leak-proof CLP/HD composites

The CLP/HD composites were produced at different weight combinations by vacuum technique. The HD was firstly melted at 40 °C and then blended with specific amount of CLP powder into a beaker. This sol-gel was mixed 30 min using a mechanical stirrer and then vacuum process was adopted to increase the impregnation ratio of the PCM using a vacuum pump integrated-oven. This process was repeated at 40 °C for 60 min by changing the impregnation weigh fraction of HD from 40 to 75 wt%. To decide the optimal HD impregnation rate into CLP, the leakage controlling test was adopted to each composite sample. The sample on a filter paper was weighed before the test and then maintained at 40 °C for 60 min. The apparent outflow case from the sample to the surface of filter paper was checked after heat treatment. By considering the weight loss related with outflow of melted HD, the final impregnation rate of HD was determined. Based on the test results, the prepared composite including 70 wt% HD was defined as leak-proof composite PCM.

2.4. Characterization techniques

The surface textural characteristics of CLP after and before HD impregnation were determined via N_2 gas adsorption-desorption method by using a surface analyzer (Gemini VII 2390 V1.03 model Micromeritics Inc.). The surface morphology of the leak-proof CLP/HD composite and its components were characterized using a SEM instrument (Zeiss LEO 440 model). The chemical functional groups of pure HD, CLP and the developed composite were identified by using FTIR spectroscopy (JASCO 430 model). The crystalline structures of the samples were carried out by XRD powder diffraction analysis at 19–23 °C using a PANalytical X'-Pert^3 model X-ray diffractometer (CuKα radiation, $\lambda = 1.542$ Å; scanning rate of 10° min^{-1}). The LHS properties of pure HD and the CLP/HD composite PCM were determined using a DSC analyzer (Hitachi 7020 model) at heating/cooling rate of 3 °C/min. Thermal stability of pure HD, CLP and the developed composite PCM were investigated using Thermogravimetric analysis (TGA) instrument (PerkinElmer model) under argon atmosphere with a heating rate of 20 °C/min. To examine the thermal reliability and chemical stability of the composite PCM, it was subjected to repeated melt/freeze cycling test using a thermal cycler device. Throughout this test, the composite sample was heated to 40 °C for 5 min and immediately after cooled to 10 °C for 5 min. After 500 and 1000 cycles, the changes in the LHS properties were estimated and the chemical structure of the composite PCM was also checked.

Thermal conductivities of the samples were measured at below and above melting temperature of HD (10 and 30 °C) using a thermal analyzer (Decagon KD2 Pro model) which works based on the transient *hot-wire method*. The measurements were repeated for three times for each sample and the data was recorded with mean deviation of ±0.010 W/m.K.

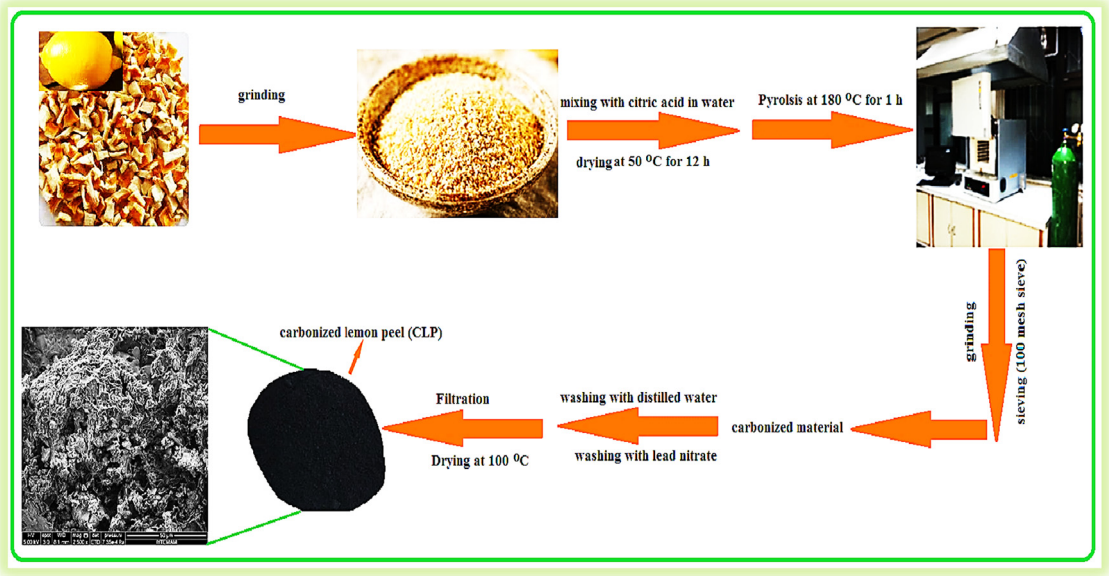

Fig. 1. Schematic demonstration of the production procedure of CLP.

To investigate the effect of the enhanced thermal conductivity on the charging/discharging periods of the leak-proof CLP/HD composite, the temperature-time histories were logged during its heating and cooling processes using the experimental design consisted with a temperature controlled-water bath, thermocouple and data logger.

The apparent densities of the CLP and the leak-proof CLP/HD composite was determined using spectrophotometer cuvettes with known volume and weight. The density of solid powder samples was determined according to the weighing difference after well placing vibration. The real densities of the CLP and the leak-proof CLP/HD composite were determined with a Quantachrome Ultrapycnometer 1000 helium pycnometer.

3. Results and discussions

3.1. Textural properties of produced CLP

The N_2 gas adsorption-desorption isotherms of the CLP and CLP/HD composite were shown in Fig. 2(a–b). The obtained surface textural properties were also presented in Table 1. The isotherm curves are in agreement with reversible Type II isotherm model according to the classification of IUPAC. As clearly seen from the tabulated data, the surface characteristics of the CLP after the HD impregnation were considerably changed. The maximum adsorption-desorption amount of the CLP at saturation was reduced from 200 cm^3/g to 38 cm^3/g after impregnation process because micropores and some mesopores was filled up by HD molecules. The BET and Langmuir surface areas of the produced CLP are 55.18 m^2/g and 72.86 m^2/g, respectively whereas they were decreased to 15.97 m^2/g and 39.83 m^2/g through loading HD, respectively. Moreover, after HD impregnation, the average pore diameter of the CLP was lessened from to 25.01 nm to 21.75 nm while its total pore volume diminished from 0.027 cm^3/g to 0.017 cm^3/g. The reductions in the above mentioned properties were due to the retention of HD molecules into the pores of the CLP. The parallel results were presented for AC after the infiltration of n-octadecane [18]. Additionally, the apparent densities of the CLP and the leak-proof CLP/HD composite were determined as 0.951 g/cm^3 and 1.087 g/cm^3, respectively while their real densities were measured as 1.704 g/cm^3 and 1.791 g/cm^3, respectively using a helium pycnometer. The increase in the real density shows that the number of open pores in the structure of the CLP is quite low and only a small portion of them was occupied with HD during the impregnation process. The HD mostly filled the intrerparticle voids rather than the open pores with limited number. The significant reduction in the BET and Langmuir surface areas also confirms this result.

3.2. Leak-proof stability and surface morphology of the developed composite PCM

The photograph images of some CLP/HD composite samples containing lower/and higher amount of HD than leak-proof weight fraction are shown in Fig. 3. As clearly observed from the photographs taken from front side and back side of the composite samples, the CLP/HD (60 wt%) and CLP/HD(65 wt%) sample showed no leakage while the sample containing 67 wt% HD demonstrated visible leakage. Therefore, the CLP/HD(65 wt%) sample was called as leak-proof composite PCM.

On the other hand, the SEM photographs of the CLP and the leak-proof CLP/HD composite are presented in Fig. 4(a-b). As demonstrated from Fig. 4(a), the surface of CLP has a partially porous structure with rough microspores with different diameters of about 5–10 μm. However, the number of open pores in the structure of CLP has is quite low. As also observed clearly from Fig. 4(b), the surface morphology of CLP was noticeably changed because HD filled the interparticle spaces on the surface rather than the open pores with limited number. Therefore, the surface tension and capillary forces between HD molecules and the particles on the surface of CLP blocked the leakage case of the molten HD from the composite.

3.3. FTIR and XRD analysis results

The FTIR spectra of CLP, HD and CLP/HD composite are depicted in Fig. 5. In the spectrum of pure HD, the distinctive peaks at 2956, 2920 and 2852 cm^{-1} are related with the stretching vibrations of C–H of groups as the bending and in-plane rocking vibrations of these bands are placed at 1466, 1373 and 729 cm^{-1} [37].

The FTIR spectrum of CLP indicates typical bands in wavenumber range of 500–1200 cm^{-1}. The bands around 1614 and 1706 cm^{-1} represents the esterified and free carboxyl groups. The broad band at 3200 and 3600 cm^{-1} shows the presence of hydroxyl groups [38]. Besides, compared to the distinguishing bands of the CLP and HD with

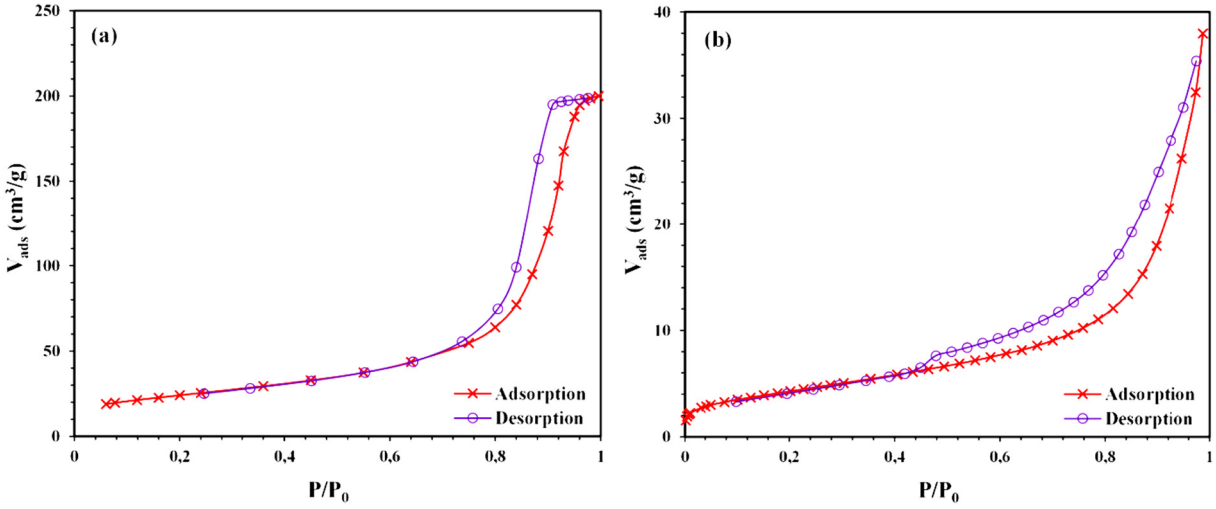

Fig. 2. Adsorption-desorption isotherms of (a) CLP and (b) CLP/HD composite.

Table 1
Surface textural properties of CLP and CLP/HD composite.

CLP		CLP/HD composite	
Characteristic	Value	Characteristic	Value
BET specific surface area (m^2/g)	55.18	BET specific surface area (m^2/g)	15.97
Micropores (m^2/g)	42.04	Micropores (m^2/g)	3.25
Mesopores (m^2/g)	13.14	Mesopores (m^2/g)	12.72
Langmuir surface area (m^2/g)	72.86	Langmuir surface area (m^2/g)	39.83
Total pore volume (cm^3/g)	0.027	Total pore volume (cm^3/g)	0.017
Micropores (cm^3/g)	0.019	Micropores (cm^3/g)	0.006
Mesopores (cm^3/g)	0.008	Mesopores (cm^3/g)	0.011
Average pore diameter (nm)	25.01	Average pore diameter (nm)	21.75

those of the prepared composite, it can be also resulted that no new band was appeared after impregnation.

The XRD diffraction patterns of pure HD, CLP and the leak-proof CLP/HD composite are indicated in Fig. 6. The XRD pattern of CLP shows a broad amorphous peak between $2\theta = 10–25°$. The presence of the minor peaks in this range is due to some degree of graphitic carbon crystallization.

The pure HD normally had two characteristic crystalline peaks at about 21° and 23° [35,39]. However, in this work, these crystalline peaks could not be observed because the HD was not in solid powder

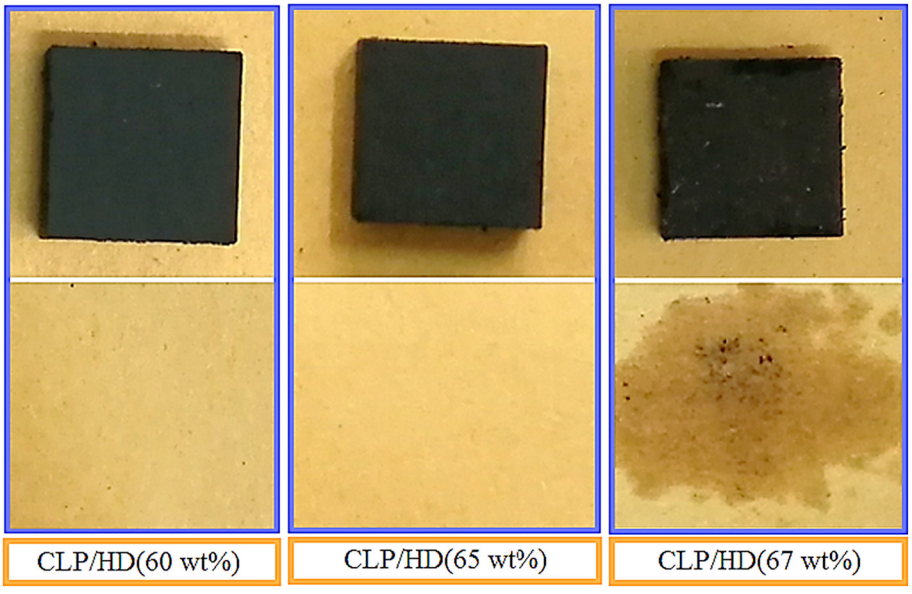

Fig. 3. Photographs of the front side and back side of leak-proof and non-leak proof CLP/HD composite.

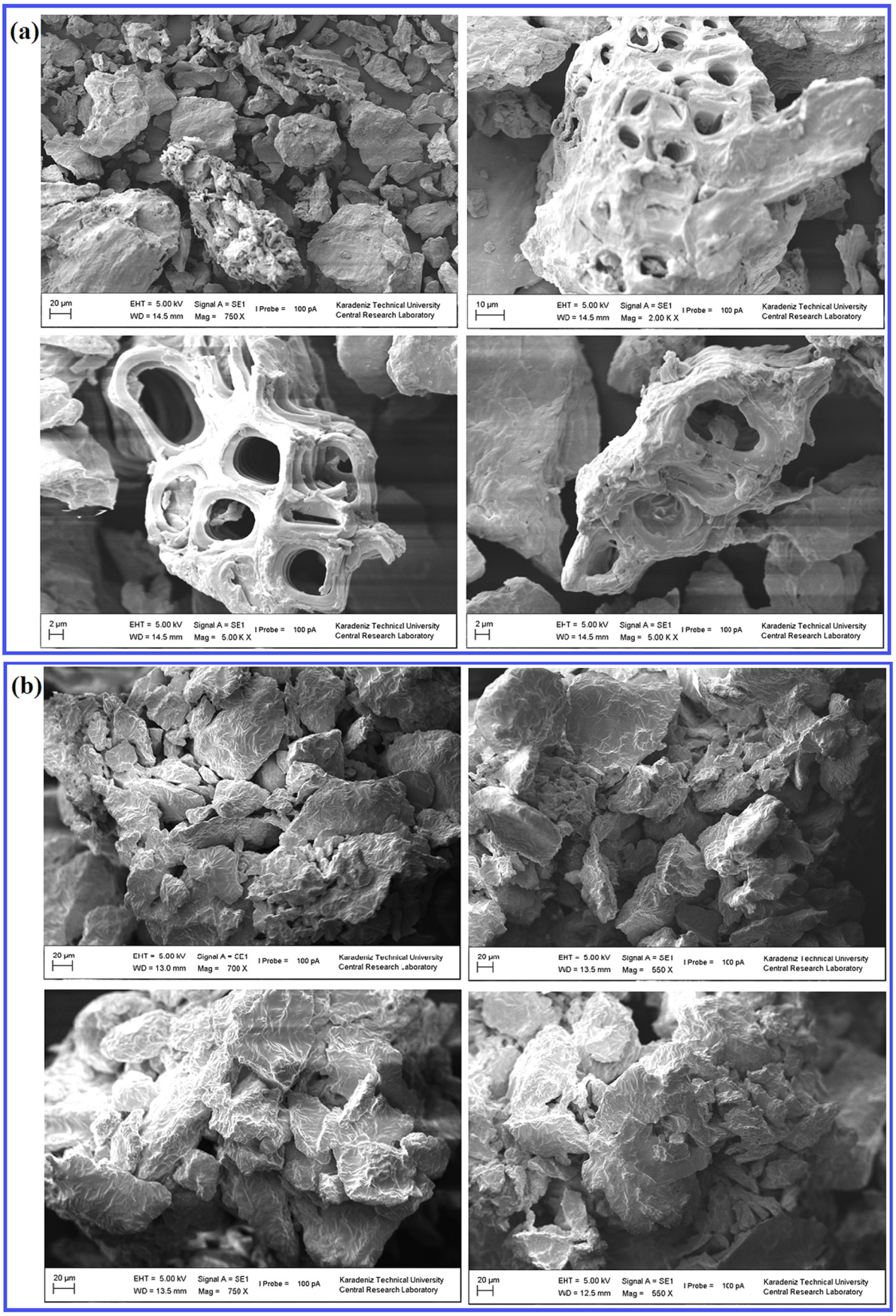

Fig. 4. SEM photographs of (a) CLP and (b) leak-proof CLP/HD.

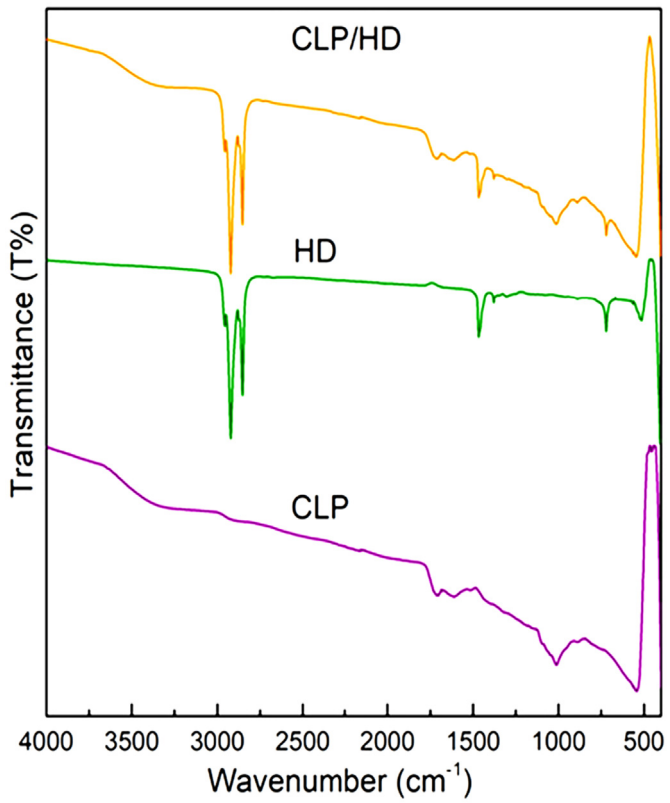

Fig. 5. FTIR results of pure HD, CLP and the leak-proof CLP/HD composite PCM.

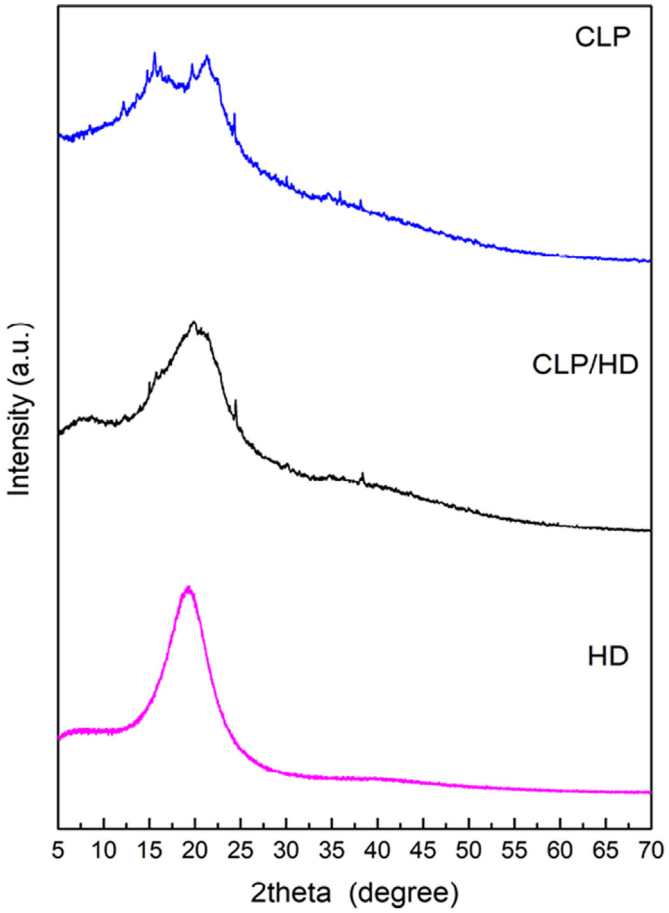

Fig. 6. XRD diffraction patterns of HD, CLP and the CLP/HD composite.

state and contrarily in melted state at examined analysis temperature (19–23 °C). Therefore, contrary to the expected typical crystalline peaks, the observed peak in the 2θ range of about 13–25° represents the non-crystallization of HD. Moreover, as seen from the diffraction patterns of the LCP/HD composite, this peak was overlapped by the broad amorphous peak of CLP. Consequently, the XRD results indicated that that HD was incorporated with the CLP matrix with no chemical interactions [18,19,30].

3.4. LHS properties of the developed CLP/HD composite

The DSC curves obtained for pure HD and the leak-proof CLP/HD composite PCM were presented in Fig. 7a. As clearly seen from the thermograms, the heating and cooling thermal behavior of the composite PCM is very similar to that of pure HD. The solid-solid phase transition and melting temperature of pure HD was measured as 9.36 °C and 19.86 °C, respectively.

Similarly, the leak-proof CLP/HD composite PCM showed the corresponding phase change peaks at 9.30 °C and 19.79 °C, respectively. The melting LHS capacities of pure HD and composite PCM were determined as 219.1 and 141.8 J/g, respectively. The rate of the LHS values (64.7%) is very close to the weigh fraction (65.0%) of HD impregnated with the CLP. Moreover, as evidently seen from Table 2, the CPL/HD composite PCM had higher melting LHS capacity than that of several bio-waste derived carbon/PCM composite PCMs in literature [11,20–22,25,26,40–43].

3.5. Cycling LHS reliability and chemical structure stability of the developed CLP/HD composite

The leak-proof CLP/HD composite PCM was subjected to 1000 accelerated melting/freezing cycles to assess its cycling reliability/and stability in its LHS properties and chemical structure. The obtained cycling DSC results were demonstrated in Fig. 8. The melting temperature of the composite PCM was slightly changed by 0.02 °C and 0.03 °C, respectively after 500th and 1000th cycle while the reduction in its melting LHS capacity is less than 1% after 1000 cycles, meaning that the CLP/HD composite PCM had good cycling LHS reliability through the melt/freeze cycles repeated for 1000 times.

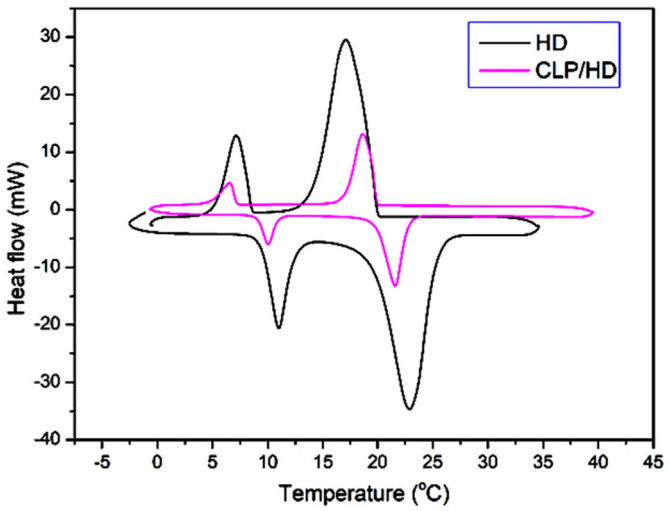

Fig. 7. DSC curves of pure HD and the CLP/HD composite PCM.

Table 2
Comparison of melting LHS capacity measured for the CLP/HD composite PCM with those of various bio-char based composite PCMs.

Waste material used for biochar precursor	PCM	Melting LHS capacity (J/g)	Reference
Rice husk	Palm wax	92.13	[11]
	Soy wax	83.91	
Pepper straw	Palmitic acid	95.50	[20]
Palm kernel shell	n-Octadecane	87.42	[21]
Peat soil	n-Octadecane	107.2	[22]
Sewage sledge biochar	Dodecanol	73.7	[25]
Oilseed straw biochar	Dodecane	90.5	
Coconut shell	PEGs	81.30–90.20	[26]
Abandoned rice	Palmitic-Lauric acid	135.4	[40]
Pinecone biochar	Palmitic acid	84.7	[41]
PEFC-certified spruce feedstock	Dodecane	77.20	[42]
	Tetradecane	67.90	
	Octadecane	91.50	
Activated waste walnut shell	Methyl palmitate	138.12	[43]
Waste lemon peel	Heptadecane (HD)	141.8	*This study*

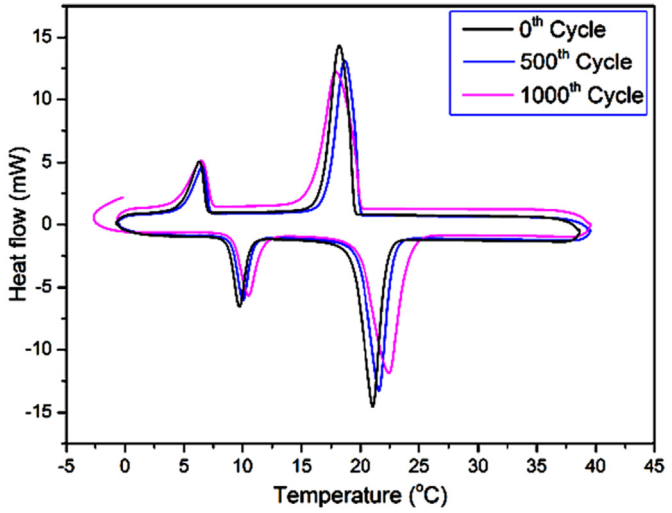

Fig. 8. DSC curves of the CLP/HD composite PCM obtained at 0th, 500th and 1000th cycle.

On the other hand, the FTIR spectrums of the leak-proof CLP/HD composite PCM taken for 0th, 500th and 1000th cycle are presented in Fig. 9. As obviously seen from the spectrums, the foremost absorption bands were not undergone any shape distortion while they were recorded at the same wavenumber values. This result confirmed that the chemical structure of the prepared CLP/HD composite PCM was protected after 1000 thermal cycles.

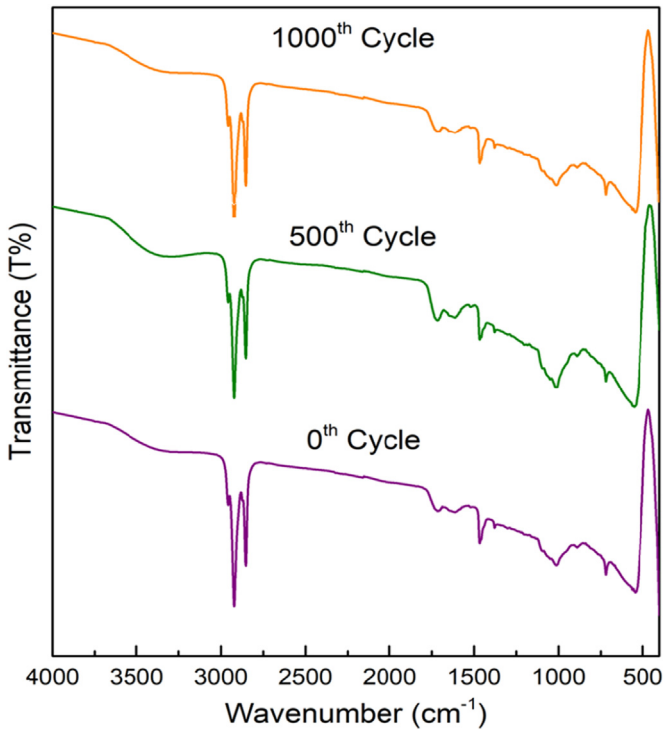

Fig. 9. FTIR spectrums of the composite PCM obtained at 0th, 500th and 1000th cycle.

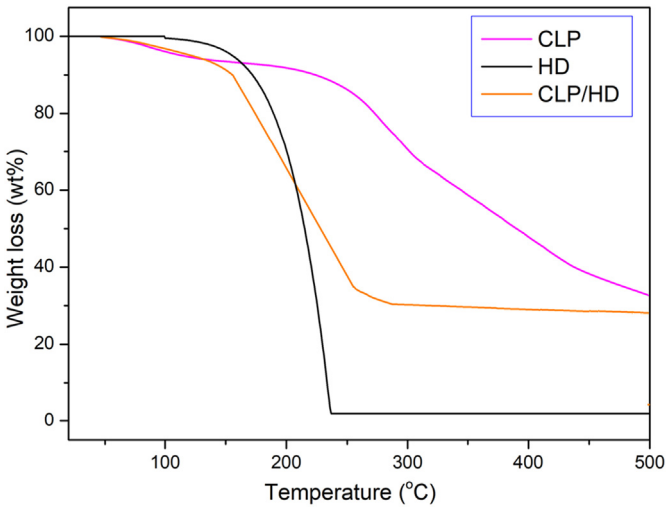

Fig. 10. TG analysis curves of pure HD, CLP and the leak-proof composite PCM.

3.6. Thermal degradation stability results

Thermal degradation temperatures of pure HD, CLP and leak-proof CLP/HD composite were determined by TGA technique and the obtained results were shown in Fig. 10. The HD was decomposed at the temperature range of 147–237 °C with residual mass of 2.3 wt% at 500 °C. The thermal degradation of the CLP at about 110 °C is corresponding to the evaporation of water (3.6 wt%) maintained into the porous structure of CLP despite of drying process. Over this temperature, the weight loss process is due to thermal decomposition of its organic ingredients.

On the other hand, the leak-proof CLP/HD composite PCM shows two decomposition steps, the first one at about 110 °C is associated with removal of water content belongs to the CLP while the second step between 110 °C and 254 °C is related with the evaporation of HD, which is represented by weight loss of 64.7 wt%. Consequently, it can be evident that the second decomposition step of the composite PCM is started much more above its phase change working temperature (about 20 °C). This result also means that and the developed composite PCM has appreciated thermal degradation stability.

3.7. Comparison of thermal conductivity values and of phase change times of pure HD and the CLP/HD composite

Thermal conductivity is one of the basic features which significantly influence the heat charging and discharging duration of a PCM. Within this framework, thermal conductivity values of pure HD, CLP and the

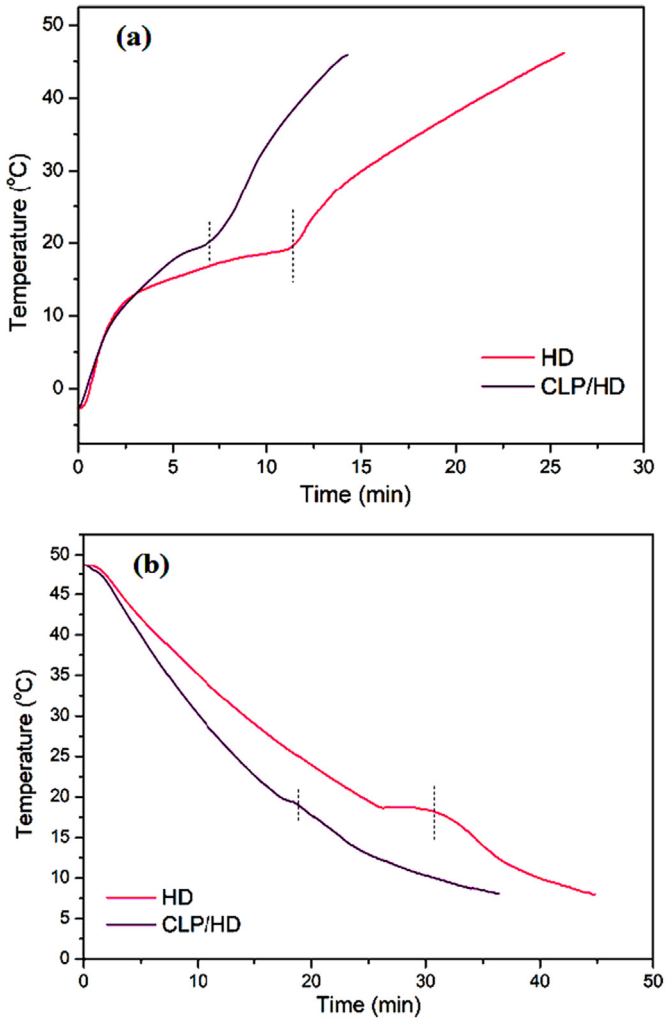

Fig. 11. Comparison of the phase change times of pure HD and CLP/HD composite PCM.

CLP/HD composite were measured as 0.26 0.84 and 0.46 W/m.K, respectively at 10 °C which is below the solidification temperature of HD. Considering these data, it can be inferred that the thermal conductivity of the CLP/HD composite was 77% higher than that of HD. It was due to the heat transfer channels and heat conduction framework provided by the carbon skeleton of CLP. However, contrarily o the expectation, the reason for lower thermal conductivity of the CLP/HD composite than that of CLP can be related to the following facts: (i) All of the pores was not completely filled by HD, which was confirmed by BET analysis results. Thus, there are still somewhat pores in the structure of the composite CLP, which are occupied with air molecules with low thermal conductivity (0.026 W/m.K). (ii) The surface area of the CLP was decreased after HD impregnation. (iii) The CLP surface is covered by HD which has approximately 4 times lower thermal conductivity than its own value. Furthermore, the thermal conductivity of pure HD and the composite PCM was measured as 0.34 and 0.61 W/m.K, respectively at 30 °C, which is above the melting temperature of HD. This result showed that the thermal conductivity of pure HD and *CLP*/HD composite has considerably boosted during the melting state. The similar findings were reported for solid and melted states of different pure PCMs and their composite PCM [18,19,28,29].

Additionally, the thermal conductivity of the CLP/HD composite PCM is at comparable level with those of different bio-char based composite PCMs. The thermal conductivity value was reported as 0.40 and 0.35 W/m.K for carbonized kapok included erythritol and mannitol, respectively [44]. The thermal conductivity of rice based biochar/palmitic-lauric acid composite was measured as 0.44 W/m.K [45]. Besides, it was determined as 0.33 W/m.K for the carbonized sunflower straw/stearic acid [31] and 0.43 W/m.K for of carbonized cotton/paraffin wax composite PCM [40].

On the other hand, the impact of the boosted thermal conductivity on the melting and solidification times of the leak-proof composite PCM was also indicated in Fig. 11.

The considered melting/and solidification times were demonstrated by dotted lines. The melting times for pure HD and the composite PCM were found as 11 and 6 min, respectively while their solidification times were found as 31 and 19 min, respectively. These findings showed that melting and solidification time of the CLP/HD composite was reduced by about 83% and 63%, respectively relative to pure HD due to the enhanced thermal conductivity.

4. Conclusions

Waste lemon peels were carbonized and then evaluated to create a novel leak-proof composite PCM for TES implementations. The HD was successfully integrated with the obtained CLP framework in the mass faction of 65% without detecting PCM leakage issue. The SEM results showed that the pores structure of the CLP would allow easily and homogenous impregnation of molten HD. The FTIR and XRD analysis proved that any chemical reaction was not involved in the incorporation of HD with the CLP. The DSC measurements revealed that the developed leak-proof composite PCM had a melting temperature of 19.79 °C and LHS capacity of 141.8 J/g. The cycling DSC findings demonstrated that the composite PCM had well thermal stability after a 1000 heating-cooling treatment. The TGA data indicated that the fabricated composite PCM has considerable high thermal degradation stability. The thermal conductivity of the composite PCM (0.46 W/m.K at 10 °C) was approximately 77% higher than that of HD (0.26 W/m.K at 10 °C). Accordingly, the developed CLP/HD composite PCM can be considered as cost-effective and eco-friendly admixture for producing innovative energy saving-construction materials used for thermal management of buildings.

Declaration of Competing Interest

The authors declare that they have no conflict of interest.

References

[1] S. Arunachalam, Latent heat storage: container geometry, enhancement techniques, and applications-A Review, J. Sol. Energy Eng. 141 (5) (2019) 050801.
[2] C. Yadav, R.R. Sahoo, Experimental analysis for optimum thermal performance and thermophysical parameters of MWCNT based capric acid PCM by using T-history method, Powder Technol. 364 (2020) 392–403.
[3] A. Sarı, A. Bicer, C. Alkan, A.N. Özcan, Thermal energy storage characteristics of myristic acid-palmitic eutectic mixtures encapsulated in PMMA shell, Sol. Energy Mater. Sol. Cells 193 (2019) 1–6.
[4] B.B. Paulo, K. Andreola, O. Taranto, A.D. Ferreira, A.S. Prata, Coating approach for a phase change material (PCM), Powder Technol. 341 (2019) 147–156.
[5] R. Methaapanon, S. Kornbongkotmas, C. Ataboonwongse, A. Soottitantawat, Microencapsulation of n-octadecane and methyl palmitate phase change materials in silica by spray drying process, Powder Technol. 361 (2020) 910–916.
[6] K. Kant, A. Shukla, A. Sharma, Advancement in phase change materials for thermal energy storage applications, Sol. Energy Mater. Sol. Cells 172 (2017) 82–92.
[7] W. Ji, X. Cheng, Si Chen, X. Wang, Y. Li, Self-assembly fabrication of GO/TiO2@paraffin microcapsules for enhancement of thermal energy storage, Powder Technol. 385 (2021) 546–556.
[8] K. Liang, L. Shi, J. Zhang, J. Cheng, X. Wang, Fabrication of shape-stable composite phase change materials based on lauric acid and graphene/graphene oxide complex aerogels for enhancement of thermal energy storage and electrical conduction, Thermochim. Acta 664 (2018) 1–15.
[9] G. Ma, J. Sun, Y. Zhang, Y. Jing, Y. Jia, Preparation and thermal properties of stearic acid-benzamide eutectic mixture/expanded graphite composites as phase change materials for thermal energy storage, Powder Technol. 342 (2019) 131–140.
[10] X. Cheng, G. Li, G. Yu, Y. Li, J. Han, Effect of expanded graphite and carbon nanotubes on the thermal performance of stearic acid phase change materials, J. Mater. Sci. 52 (2017) 12370–12379.

[11] J. Jeon, J.H. Park, S. Wi, S. Yang, Y.S. Ok, S. Kim, Latent heat storage biocomposites of phase change material-biochar as feasible eco-friendly building materials, Environ. Res. 172 (2019) 637–648.
[12] A. Sarı, T.A. Saleh, G. Hekimoğlu, M. Tuzen, V.V. Tyagi, Evaluation of carbonized waste tire for development of novel shape stabilized composite phase change material for thermal energy storage, Waste Manag. 103 (2020) 352–360.
[13] Y. Wang, T.D. Xia, H. Zheng, H.X. Feng, Stearic acid/silica fume composite as form-stable phase change material for thermal energy storage, Energy Build. 43 (2011) 2365–2370.
[14] H. Zhang, L. Zhang, Q. Li, C. Huang, H. Guo, L. Xiong, X. Chen, Preparation and characterization of methyl palmitate/palygorskite composite phase change material for thermal energy storage in buildings, Constr. Build. Mater. 226 (2019) 212–219.
[15] Y. Konuklu, O. Ersoy, F. Erzin, Development of pentadecane/diatomite and pentadecane/sepiolite nanocomposites fabricated by different compounding methods for thermal energy storage, Int. J. Energy Res. 43 (2019) 6510–6520.
[16] H. Zhang, J. Zhu, W. Zhou, F. Liu, K. Li, Synthesis and thermal properties of a capric acid modified expanded vermiculite phase change material, J. Mater. Sci. 54 (2019) 2231–2240.
[17] D.G. Atinafu, Y.S. Ok, H.W. Kua, S. Kim, Thermal properties of composite organic phase change materials (PCMs): a critical review on their engineering chemistry, Appl. Therm. Eng. 181 (2020) 115960.
[18] T. Khadiran, M.Z. Hussein, Z. Zainal, R. Rusli, Activated carbon derived from peat soil as a framework for the preparation of shape-stabilized phase change material, Energy 82 (2015) 468–478.
[19] T. Khadiran, M.Z. Hussein, Z. Zainal, R. Rusli, Shape-stabilised n-octadecane/activated carbon nano composite phase change material for thermal energy storage, J. Taiwan Inst. Chem. Eng. 55 (2015) 189–197.
[20] X. Gu, P. Liu, C. Liu, L. Peng, H. He, A novel form-stable phase change material of palmitic acid-carbonized pepper straw for thermal energy storage, Mater. Lett. 248 (2019) 12–15.
[21] Y. Jiang, Preparation of activated carbon from walnut shell and its application in industrial wastewater, AIP Conf. Proc. 1839 (2017), 020063.
[22] M.Z. Hussein, T. Khadiran, Z. Zulkarnain, R. Rafeadah, Properties of n-octadecane-encapsulated activated carbon nanocomposite for energy storage medium: the effect of surface area and pore structure, Aust. J. Basic Appl. Sci. 9 (8) (2015) 82–88.
[23] C. Wang, L. Feng, W. Li, J. Zheng, W. Tian, X. Li, Shape-stabilized phase change materials based on polyethylene glycol/porous carbon composite: the influence of the pore structure of the carbon materials, Sol. Energy Mater. Sol. Cells 105 (2012) 21–26.
[24] Y. Zhao, X. Min, Z. Huang, Y. Liu, X. Wu, M. Fang, Honeycomb-like structured biological porous carbon encapsulating PEG: a shape-stable phase change material with enhanced thermal conductivity for thermal energy storage, Energy Build. 158 (2018) 1049–1052.
[25] D.G. Atinafu, S.J. Chang, S. Kim, Infiltration properties of n-alkanes in mesoporous biochar: The capacity of smokeless support for stability and energy storage, J. Hazard. Mater. 399 (2020) 123041.
[26] L. Feng, J. Zheng, H. Yang, Y. Guo, W. Li, X. Li, Preparation and characterization of polyethylene glycol/active carbon composites as shape-stabilized phase change materials, Sol. Energy Mater. Sol. Cells 95 (2011) 644–650.
[27] A.F. Nicholas, M.Z. Hussein, Z. Zainal, T. Khadiran, Palm kernel shell activated carbon as an inorganic framework for shape-stabilized phase change material, Nanomaterials (Basel) 8 (2018) 689.
[28] Z. Chen, F. Shan, L. Cao, G. Fang, Synthesis and thermal properties of shape-stabilized lauric acid/activated carbon composites as phase change materials for thermal energy storage, Sol. Energy Mater. Sol. Cells 102 (2012) 131–136.
[29] W. Zhang, X. Zhang, X. Zhang, Z. Yin, Y. Liu, M. Fang, X. Wu, X. Min, Z. Huang, Lauric-stearic acid eutectic mixture/carbonized biomass waste corn cob composite phase change materials: preparation and thermal characterization, Thermochim. Acta 674 (2019) 21–27.
[30] Y. Xu, X. Zhang, B. Wu, Y. Xu, R. Wen, Y. Liu, M. Fang, X. Wu, X. Min, Z. Huang, Preparation and performance of shape-stable phase change materials based on carbonized-abandoned orange peel and paraffin, Fullerenes Nanotubes Carbon Nanostruct. 27 (2019) 289–298.
[31] R. Wen, W. Zhang, Z. Lv, Z. Huang, W. Gao, A novel composite phase change material of stearic acid/carbonized sunflower straw for thermal energy storage, Mater. Lett. 215 (2018) 42–45.
[32] A. Bhatnagar, A.K. Minocha, M. Sillanpää, Adsorptive removal of cobalt from aqueous solution by utilizing lemon peel as biosorbent, Biochem. Eng. J. 48 (2010) 1181–1186.
[33] G.R.K. Kumar, M.S. Kamath, P.S. Mallapur, Defluoridation of water by using low cost activated carbon prepared from lemon peels, J. Basic Appl. Eng. Res 3 (2016) 658–660.
[34] A. Bhatnagar, E. Kumar, A.K. Minocha, Removal of anionic dyes from water using citrus limonum (lemon) peel: equilibrium studies and kinetic modeling, Sep. Sci. Technol. 44 (2009) 316–334.
[35] S.G. Ranjbar, G. Roudini, F. Barahuie, Fabrication and characterization of phase change material-SiO_2 nanocomposite for thermal energy storage in buildings, J. Energy Storage 27 (2020) 101168.
[36] A. Sarı, C. Alkan, D. Kahraman Döğüşcü, A. Biçer, Micro/nano-encapsulated n-heptadecane with polystyrene shell for latent heat thermal energy storage, Sol. Energy Mater. Sol. Cells 126 (2014) 42–50.
[37] F. Irani, Z. Ranjbar, S. Moradian, A. Jannesari, Microencapsulation of n-heptadecane phase change material with starch shell, Prog. Org. Coat. 113 (2017) 31–38.
[38] H. Arslanoglu, H.S. Altundogan, F. Tumen, Preparation of cation exchanger from lemon and sorption of divalent heavy metals, Bioresour. Technol. 99 (2008) 2699–2705.
[39] D. Sarabandi, G. Roudini, F. Barahuie, Activated carbon derived from pine cone as a framework for the preparation of n-heptadecane nanocomposite for thermal energy storage, J. Energy Storage 24 (2019) 100795.
[40] X. Zhang, Z. Huang, Z. Yin, W. Zhang, Y. Huang, Y. Liu, M. Fang, X. Wu, X. Min, Form stable composite phase change materials from palmitic-lauric acid eutectic mixture and carbonized abandoned rice: preparation, characterization, and thermal conductivity enhancement, Energy Build. 154 (2017) 46–54.
[41] Y. Wan, Y. Chen, Z. Cui, H. Ding, S. Gao, Z. Han, J. Gao, A promising form-stable phase change material prepared using cost effective pinecone biochar as the matrix of palmitic acid for thermal energy storage, Sci. Rep. 9 (2019) 11535.
[42] D.G. Atinafu, S. Jin Chang, K.-H. Kim, S. Kim, Tuning surface functionality of standard biochars and the resulting uplift capacity of loading/energy storage for organic phase change materials, Chem. Eng. J. 394 (2020) 125049.
[43] G. Hekimoğlu, A. Sarı, T. Kar, S. Keleş, K. Kaygusuz, V.V. Tyagi, R.K. Sharma, A. Al-Ahmed, F.A. Al-Sulaiman, T.A. Saleh, Walnut shell derived bio-carbon/methyl palmitate as novel composite phase change material with enhanced thermal energy storage properties, J. Energy Storage 35 (2021) 102288.
[44] J. An, W. Liang, P.M.C. Wang, T. Chen, Z. Zhu, H. Sun, A. Li, Novel sugar alcohol/carbonized kapok fiber composites as form-stable phase-change materials with exceptionally high latent heat for thermal energy storage, ACS Omega 4 (2019) 4848–4855.
[45] N. Sheng, T. Nomura, C. Zhu, H. Habazaki, T. Akiyama, Cotton-derived carbon sponge as support for form-stabilized composite phase change materials with enhanced thermal conductivity, Sol. Energy Mater. Sol. Cells 192 (2019) 8–15.